MUON SPECTROMETER FOR E_μ = 15 TeV

H. L. Anderson
Los Alamos Scientific Laboratory, Los Alamos, NM, USA.

ABSTRACT

A superconducting air gap magnet spectrometer is described for deep inelastic muon scattering at E_μ = 15,000 GeV. It accommodates a long target with close to 100% acceptance and high resolution over most of the kinematic range. Its application in measuring the electroweak interference as a sensitive high Q^2 test of the Weinberg-Salam model is described.

1. INTRODUCTION

A muon beam at E_μ = 15 TeV will be a spectacular short distance probe. With a suitable target-spectrometer combination event rates will be appreciable up to Q^2 = 10,000 GeV^2, making distances down to 2 x 10^{-16} cm accessible. For these values of Q^2 the effect of the weak interaction will be so pronounced that it will be necessary to make measurements with both μ^- and μ^+ beams to sort out the weak from the electromagnetic effects. In fact, because of the importance of establishing the validity of electroweak theories such as the Weinberg-Salam model at these high values of Q^2, the measurement of the electroweak interference may be a principal use of such a high energy muon beam.

Undoubtedly, some experiments along this line will have already been done by the time the 20 TeV machine is built. However, it will be difficult to match an external muon beam at 15 TeV when it comes to measuring with precision the nature of the weak interaction and the structure of the nucleon.

In Table 1 we list some of the standard experiments that are done with high energy muon beams. There will be added interest at E_μ = 15 TeV because of the larger dynamic range that will then become available. The higher order effects that plague tests of QCD at lower energies will be appreciably smaller at 15 TeV. Moreover, the possibility of seeing effects of new quarks and even quark structure will be enhanced. Since QCD effects are small, it will be necessary to do the measurement with high precision. Measurements should be made with Be targets for high luminosity and with liquid hydrogen and deuterium targets to separate the effects of neutron and proton.

To carry out such measurements the spectrometer should have the following characteristics:

i) High acceptance, approaching 100% over most of the kinematic range.

ii) Accommodate a long target, ≃ 100 meters, for adequate statistics at large Q^2.

iii) High resolution in angle and momentum.

Such performance can be obtained with a magnetic spectrometer having a 100 meter target inside the magnetic field and instrumented with an array of

Table 1

Experiments With High Energy Muons

1.	Electro-Weak Interference
2.	Double γ Exchange
3.	$F_2(x,Q^2)$ $100 \leq Q^2 \leq 10{,}000$ GeV^2 See if $F_2(x,Q^2)$ rises at low x and falls at high x with Q^2.
4.	Measure R
5.	Better Moments $M(n,Q^2) = \int x^{n-2} F_2(x,Q^2)\,dx$ "Test QCD"
6.	Check if $M^N(n,Q^2) \to M^P(n,Q^2)$
7.	Low x Behavior; New Quarks, Quark Structure??
8.	Multi-Muons
9.	Quark and Gluon Jets
10.	Weak Charged Current Processes
11.	Surprises?

time projection chambers having a time resolution of 1 nanosecond and a spatial resolution of 100 microns. The long target is needed because the large values of Q^2 that become possible at 15 TeV have low cross-sections. However, since scattering angles are small we can work with a magnet of small aspect ratio. Our magnet is very long, 150 meters, compared to 80 cm x 80 cm for the width and height of its useful magnetic field.

Such arrangements have been used before. The CERN muon scattering experiment NA-4 uses a 50 meter long liquid hydrogen target surrounded by a toroidal iron magnet. This spectrometer was specially designed to measure high Q^2 scattering. However, such iron magnets are not suitable if precision is important because multiple scattering in the iron limits the resolution obtainable in angle and momentum. The problem is aggravated for the high muon energies to be measured here because the critical energy for muons in iron is 870 GeV. Above this value energy loss by radiation exceeds that by ionization. Since the radiative losses in single collisions can be quite large they are more difficult to correct for. For accurate work it is better to measure angles and momenta in an air gap magnet.

2. QUARK DISTRIBUTIONS

Our calculations are based on quark momentum distributions obtained by extrapolating a Buras & Gaemers[1] type fit of current muon and electron scattering data in the range $2 \leq Q^2 \leq 200$ GeV^2 to $Q^2 = 15{,}000$ GeV^2. Figure 1 shows the quark momentum distribution at $Q^2 = 50$, 500 and 15,000 GeV^2. The calculations were made in leading order in QCD without allowance for higher order effects or for quark flavors beyond charm.

Figure 2 shows the structure function $F_2(x,Q^2)$ per nucleon for deuterium (average of proton and neutron) up to $Q^2 = 15{,}000\ GeV^2$, obtained from the extrapolated quark distributions. These were adjusted to fit the data at low Q^2 without taking higher order effects into account. The high Q^2 values will be flawed for this reason. It is just the uncertainty in dealing with the higher order effects that makes measurements at high Q^2 so valuable.

It is important to note that departures from scaling, the Q^2 variation of F_2 at constant x, are small except at large x. Measurements over a wide range of Q^2 are important if these QCD effects are to be established in a less ambiguous way. The effects at high x are larger, but the event rates are lower. In general, QCD effects tend to favor low x processes at the expense of high x. It will be interesting to see how well the experiments bear out these general rules.

3. EFFECT OF RESOLUTION

Figure 3 is shown to emphasize the importance of high acceptance and high resolution in the measurement. The cross-section has a steep dependence on both energy and angle. The number of events shown in the figure have been calculated for an integrated luminosity of 10^{40} μ's x nucleons/cm^2 by integrating over bins with $\Delta x = \Delta y = 0.2$. If the cross-sections were flat the result would be insensitive to the shape and width of the resolution function. However, in our case the dependence is very steep and a precise knowledge of the resolution function and the acceptance is required to take proper account of the overpopulation of events of small angle and low energy in the bin. The width of the resolution functions brings such events into the bin in greater number than it takes away. Even if the acceptance and resolution function were precisely known and properly accounted for there is still a reduction in the statistical accuracy of the measurement because of the way the events are redistributed over the bins.

4. ELECTROWEAK INTERFERENCE

At $E_\mu = 15$ TeV, the effects of the electroweak interactions are so large that they dominate the cross-section over a large part of the kinematic range. In the μ^+ beam coming from the π^+ decaying in the forward direction, the μ^+ is predominantly left hand polarized. For such muons the electroweak effect in the Weinberg-Salam model reduces the single photon exchange cross-section substantially over most of the kinematic range. In Figure 4, the ratio of the single photon exchange cross-section with and without the electroweak effect has been calculated[2] using the Weinberg-Salam model with $\sin^2 \theta_W = 0.21$. The ratios are shown for right and left handed μ^+ and μ^- beams. It is seen that the electroweak interference effect can increase or decrease the single photon exchange cross-section by a factor of 2 or more.

5. ELECTROWEAK INTERFERENCE EXPERIMENT

As an example of what could be done with such a spectrometer in a measurement of the electroweak interference effect, we have calculated the μ^-/μ^+ ratio of events in bins with $\Delta x = \Delta y = 0.2$, taking $\sin^2\theta_W = 0.21$. We assumed an integrated luminosity of 10^{40} muons x nucleons/cm^2. Such a luminosity can be obtained by running 10^6 μ's/second for 10^6 seconds with a 100 meter Be target. We assumed that the μ^+ beam is 90% left handed (10% right handed) and the μ^- beam 90% right handed (10% left handed) as is typical for muon beams obtained from pions decaying in the forward direction. Since μ^- beams may be several times less intense than μ^+ beams, more running time would have to be allocated to μ^- than to μ^+. The calculation assumes 100% acceptance for muons scattered in the range $2 \leq \theta \leq 30$ mrad. To assure this the spectrometer magnet is extended 50 meters beyond the end of the 100 meter target for angle and momentum measurement of muons scattered from the downstream end of the target.

Results of the calculation are shown in Figure 5 and tabulated in Table 2. Note the large number of events in the bins of low x where the ratio μ^-/μ^+ is low, and the paucity of events in high x, high y bins, where the ratio μ^-/μ^+ is high. No allowance is made for the effect of finite resolution in the measurement of angles and muon momenta, or for radiative effects which would have to be corrected for. Such an experiment measures the Weinberg angle with a statistical error $\delta\sin^2\theta_W = 0.005$.

The two photon exchange process could give an appreciable asymmetry in a μ^-/μ^+ comparison. The estimate given by Bartels[3] indicates a 10-15% effect. It should be possible to isolate the photon double exchange effect because of its different dependence on Q^2.

6. SUPERCONDUCTING MAGNETIC SPECTROMETER

A cross-section through the spectrometer magnet is shown in Figure 6. The iron yoke is from the Cosmotron magnet and is 2.4 m across the flats. The useful aperture is 80 cm x 80 cm and can operate up to 20,000 gauss with a highly uniform magnetic field. The superconducting coils are inside a 15 cm thick cryostat jacket. A space allowance of 10 cm top and bottom is provided for the time projection chamber wires and readout. A beryllium target 10 cm x 10 cm is shown as it would be used in the electroweak interference experiment. This would be replaced by liquid hydrogen and deuterium targets of 10 cm diameter for structure function determinations.

Figure 7 shows a longitudinal view of the spectrometer. There are 24 magnet modules each 6 meters long. The Be target used for the electroweak interference experiment runs through the first 16 magnets. Eight additional magnets at the far end are used to measure the small angle muons from the downstream portion of the target. The iron yoke serves as a muon identifier and is equipped with scintillation counters and drift chambers. The

Table 2

Expected number of events for an integrated luminosity of 10^{40} muons x nucleons/cm^2 at E_μ = 15,000 GeV. Calculated with polarizations 90% μ_L^+, 90% μ_R^- for $\sin^2\theta_W = 0.21$.

y=0.2-0.4 x	θ_{min} mrad	θ_{max} mrad	Events μ^+	Events μ^-	Ratio*
0.0-0.2	2.0	4.1	384610	403090	1.0480 (23)
0.2-0.4	2.5	5.8	53601	61495	1.1473 (68)
0.4-0.6	3.5	7.1	5527	6931	1.254 (23)
0.6-0.8	4.3	8.2	507	671	1.324 (78)
0.8-1.0	5.0	9.1	13	18	
y=0.4-0.6 x					
0.0-0.2	2.0	6.1	592570	622430	1.0504 (19)
0.2-0.4	4.1	8.7	12032	17754	1.476 (17)
0.4-0.6	5.8	10.6	1138	2071	1.820 (67)
0.6-0.8	7.1	12.3	99	201	2.03 (25)
0.8-1.0	8.2	13.7	2	5	
y=0.6-0.8 x					
0.0-0.2	2.0	10.0	889110	922810	1.0379 (15)
0.2-0.4	6.1	14.1	4123	8345	2.024 (38)
0.4-0.6	8.7	17.3	350	998	2.86 (18)
0.6-0.8	10.6	20.0	29	97	3.36 (71)
0.8-1.0	12.3	22.4	1	3	
y=0.8-1.0 x					
0.0-0.2	2.0	30.0	1444500	1478800	1.0238 (12)
0.2-0.4	10.0	30.0	1576	4180	2.653 (78)
0.4-0.6	14.1	30.0	107	444	4.14 (45)
0.6-0.8	17.3	30.0	7	37	5.0 (2.0)
0.8-1.0	20.0	30.0		1	

*Statistical error in last two significant figures in parentheses.

scintillation counters produce a trigger for muons that have penetrated an appreciable thickness of iron and are moving outward in the iron; the drift chambers point the scattered muon back to the vertex. Precision measurements of momentum and angle are obtained with time projection chambers that operate in the 20,000 gauss magnetic field. The muon identifier at the end is for small angle scattered muons which have not penetrated a sufficient length of magnetic yoke.

7. FLASH ENCODER READOUT

The flash encoder makes possible 1 ns time resolution and 100 μm space resolution with the time projection chamber. The flash encoder made by TRW, model number TDC1007J, is an 8-bit fully parallel A/D converter capable of digitizing an analog signal every 40 ns. It has 255 sampling comparators, and if this is followed by a 512-step 8-bit shift register 20 microseconds of pulse height data can be stored and then read out to a computer if desired.

The sketch indicates how the electron avalanche at the sense wire induces charge among a series of pads. The flash encoder records the shape of each pulse by digitizing the height of a sample every 40 nanoseconds.

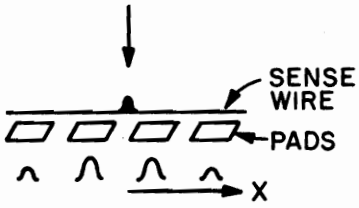

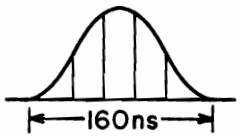

The first moment of the time distribution can be obtained to a fraction of 40 nanoseconds, or about 1 nanosecond. The space resolution is obtained from the first moment of the charge induced in the array of pads underneath the sense wire. We use one flash encoder for each pad and integrate the 40 nanosecond samples to get the total charge induced on each pad.

For precise timing we use a pair of time projection chambers as shown in the sketch, one with electrons drifting up, the other with drift down. The trigger provides the start time for the flash encoder clock. By measuring t_1 and t_2 for up and down drifted electrons we measure the location of the track $y = (t_1 - t_2)/(t_1 + t_2)$ and also the drift velocity in the chamber. Tracks that are out of time will give the wrong $t_1 + t_2$. Since the drift velocity in the argon-CH_4 mixture commonly used is 5 cm/μs, a 1 ns measurement corresponds to 50 μm in y.

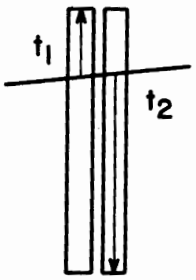

8. TIME PROJECTION CHAMBER

Time projection chambers can handle a high multiplicity of tracks. A cluster of tracks that traverse the time projection chamber simultaneously are read out sequentially as the electrons from the ion pairs they produce arrive at the sense wire. In our application the tracks are almost normal to the drift plane. Electric and magnetic field are parallel to the drift plane. The high magnetic field constrains the lateral diffusion of the electrons over the drift path. For each track the readout gives the x, y, and z coordinates of a segment of the track so that a multi-track event can be reconstructed without ambiguity. However, the presence of an excessive number of positive ions from

particles traversing the chamber previous to the triggered event could distort the electric field appreciably. To prevent this, positive ion production has to be suppressed by suitable gating on the grid wires of the chamber except following a trigger.

ACKNOWLEDGEMENT

We thank Robert J. McKee for computing most of the curves presented here.

* * *

REFERENCES

1) A. J. Buras and K. J. F. Gaemers, Nuc. Phys. B132, 249 (1978).

2) J. Ellis, *in* "CHEEP, An e-p Facility in the SPS," CERN 78-02 (1978), p. 7.

3) J. Bartels, Nuc. Phys. B82, 172 (1974).

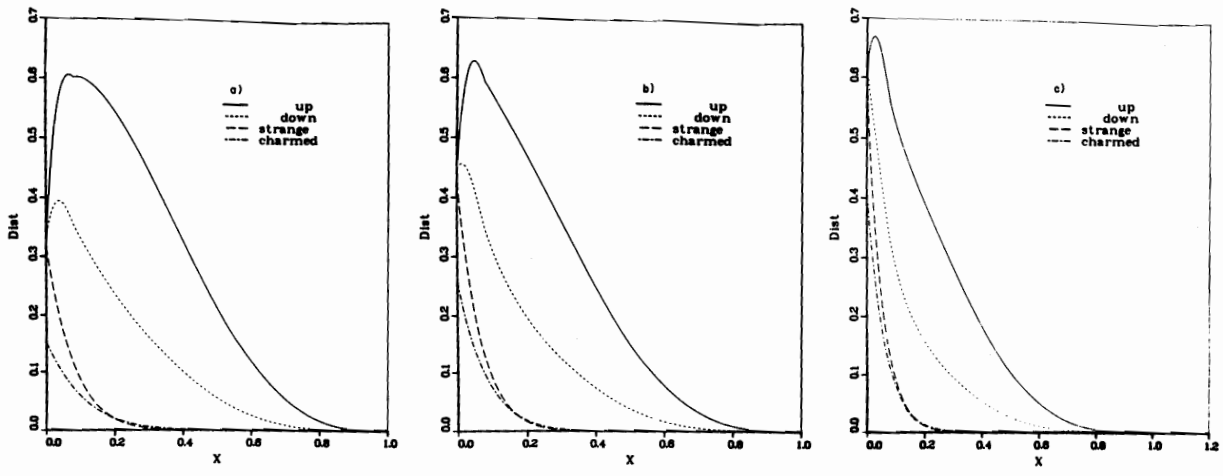

Fig. 1
a) Quark momentum density distributions at Q^2 = 50 GeV^2 as deduced from a fit of the current set of structure function measurements from SLAC, Fermilab and CERN, including the CDHS neutrino data. We used the procedure of Buras and Gaemers in obtaining a set of quark and gluon distribution functions which satisfy QCD and fit the data. b) Extrapolation to 500 GeV^2. c) Extrapolation to 15,000 GeV^2: Note the rise at small x, the fall at high x.

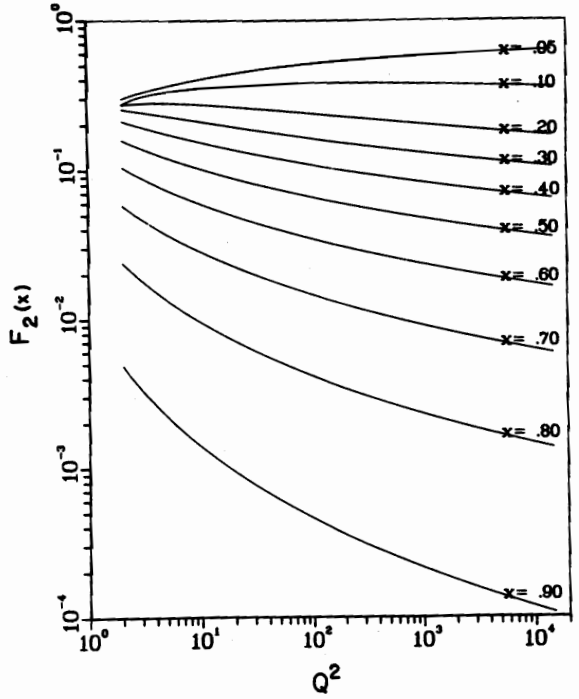

Fig. 2
The structure function $F_2(x,Q^2)$ per nucleon for deuterium, for various values of Q^2 up to Q^2 = 15,000 GeV^2, taking QCD effects into account in the manner of Buras and Gaemers, based on a fit to the data in the range $2 \leq Q^2 \leq 200$ GeV^2.

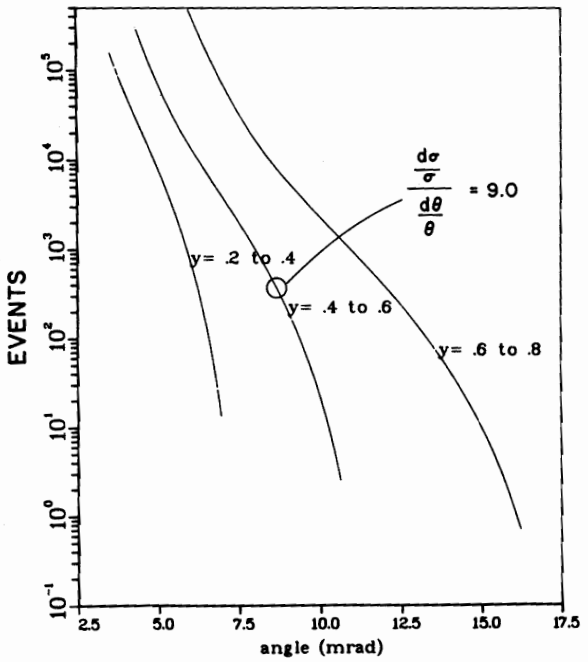

Fig. 3
Number of events expected from single photon exchange at E_μ = 15,000 GeV as a function of scattering angle for various values of $y = \nu/E$. The rates are calculated for bins with $\Delta x = 0.2$, $\Delta y = 0.2$ and total luminosity 10^{40} muons x nucleons/cm . The steep dependence of the scattering angle emphasizes the importance of precise measurement of the scattering angle. At the circled point the fractional error in the cross-section we want to measure is 9 times the uncertainty in the measurement of the scattering angle.

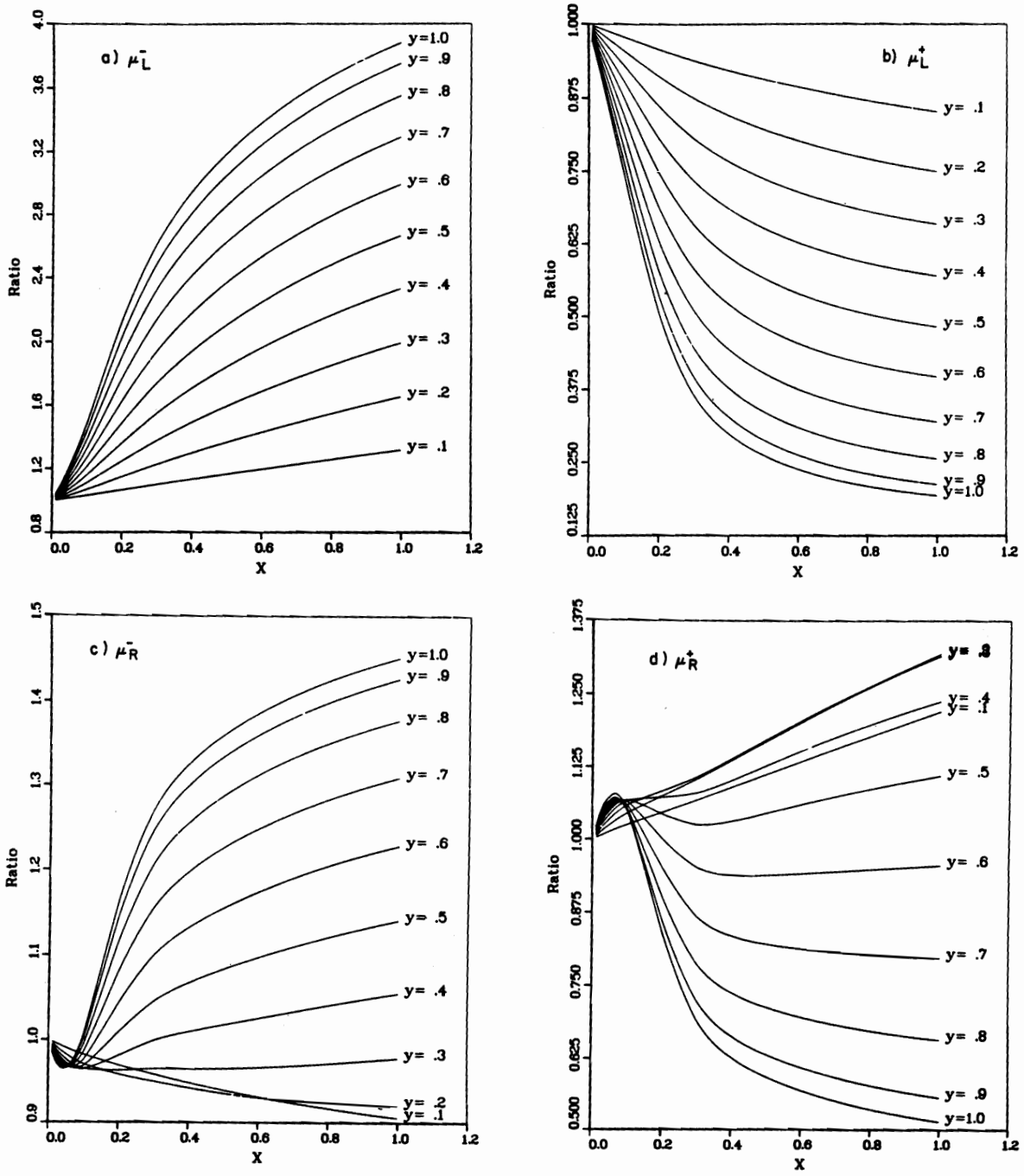

Fig. 4
Plots of the ratio total to single photon exchange cross-sections for μ^- and μ^+ with left and right handed polarization for E_μ = 15,000 GeV. The calculation of the total cross-section is based on the Weinberg-Salam model with $\sin^2\theta_W = 0.21$.

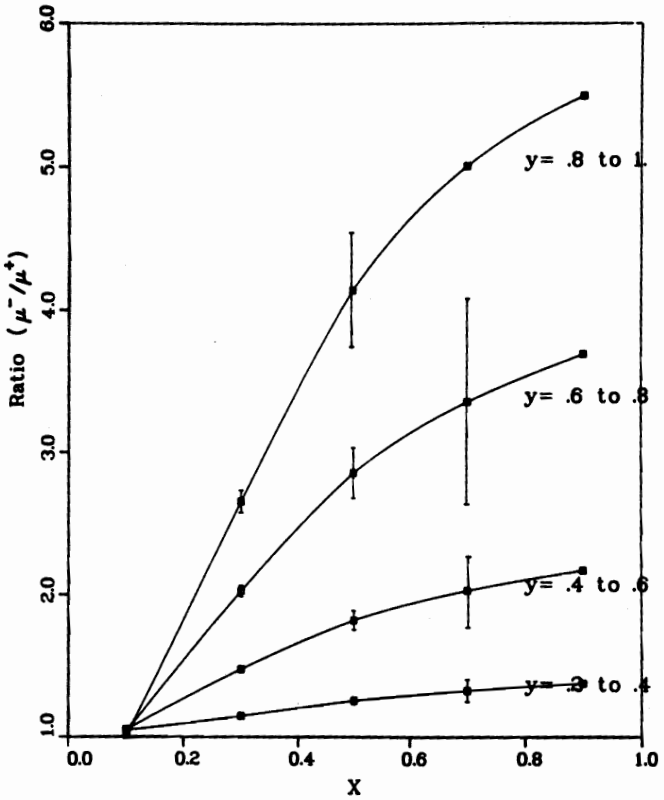

Fig. 5
Expected ratio of counts in bins with $\Delta x = 0.2$, $\Delta y = 0.2$ for μ^- and μ^+ based on the Weinberg-Salam model, $\sin^2\theta_W = 0.21$. The integrated luminosity for each sign is 10^{40} muons x nucleons/cm^2 at E_μ = 15,000 GeV. The large error bars for the highest x points on each curve have been suppressed. The point at x = 0.1 is a high statistics point which should show little asymmetry and can be used as a check against systematic errors. Radiative corrections and the effect of double photon exchange were not included in this calculation. The Weinberg angle can be determined to an uncertainty $\delta\sin^2\theta_W = 0.005$ (statistical).

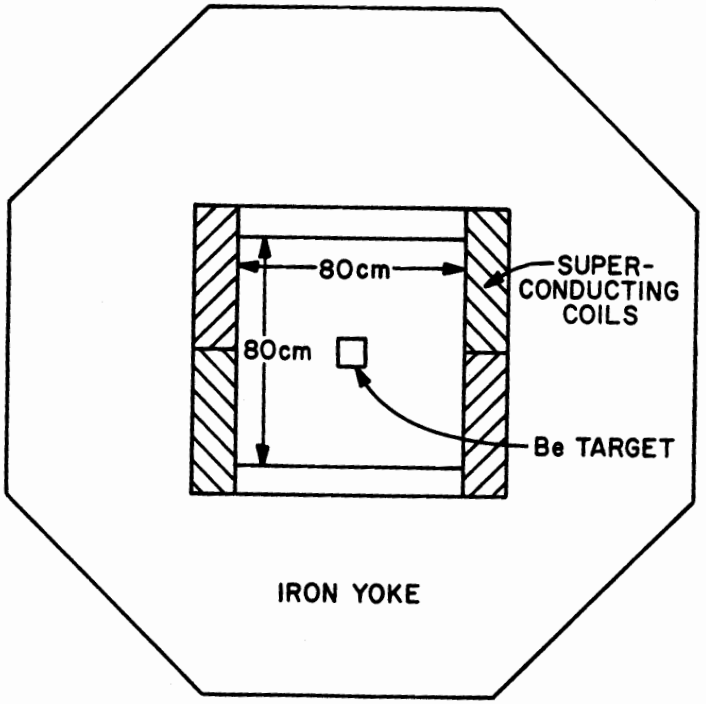

Fig. 6.
Cross-section through the superconducting air gap spectrometer. The iron yoke is from the Cosmotron magnet, 2.4 m across the flats. The useful aperture is 80 cm x 80 cm and has a highly uniform 20,000 gauss field. The superconducting coils are inside a 15 cm thick cryostat jacket; 10 cm top and bottom are for the time projection chamber readouts. A beryllium target will be used for the electroweak interference experiment.

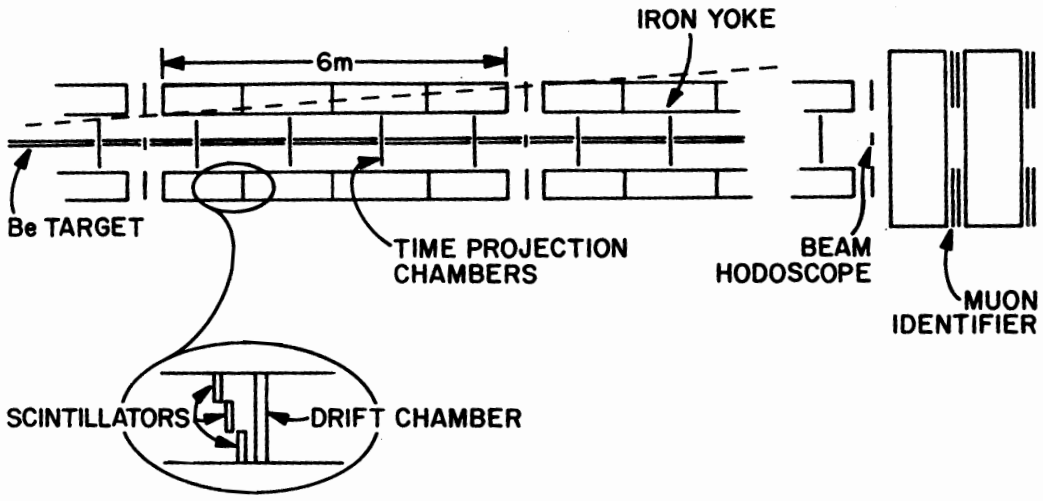

Fig. 7
Longitudinal view of superconducting air gap spectrometer. There are 24 magnet modules each 6 meters long. The Be target used for the electroweak interference experiment runs through the first 16 magnets. Eight additional magnets at the far end are used to measure the small angle muons from the downstream end of the target. The iron yoke serves as a muon identifier and is equipped with scintillation counters and drift chambers. The scintillation counters produce a trigger for muons that have penetrated an appreciable thickness of iron and are moving outward in the iron; the drift chambers point the scattered muon back to the vertex. Precision measurements of momentum and angle are obtained with time projection chambers that operate in the 20,000 gauss magnetic field. The muon identifier at the end is for small angle scattered muons which have not penetrated the magnet yoke sufficiently.